*MRS Communications (2022) 12:409–414*

https://doi.org/10.1557/s43579-022-00189-2

MRS Communications

Research Letter

# Zinc oxide films deposited on FTO substrate by hydrothermal microwave-assisted method

**Graziela de Souza, and Luís Henrique Nery,** Universidade Federal de Alfenas (UNIFAL), Rodovia José Aurélio Vilela, 11.999, Poços de Caldas, MG 37715-400, Brazil
**João Otávio D. Malafatti,** Nanotechnology National Laboratory for Agriculture (LNNA), Embrapa Instrumentação Agropecuária, Rua XV de Novembro, 1452, São Carlos, SP 13560-970, Brazil
**Jeferson Almeida Dias,** Instituto de Ciência, Tecnologia e Inovação (ICTIN), Universidade Federal de Lavras (UFLA), Aquenta Sol, São Sebastião do Paraíso, MG 37950000, Brazil
**Elaine Cristina Paris,** Nanotechnology National Laboratory for Agriculture (LNNA), Embrapa Instrumentação Agropecuária, Rua XV de Novembro, 1452, São Carlos, SP 13560-970, Brazil
**Rodolfo Foster Klein-Gunnewiek,** Universidade Federal de São Carlos, Rodovia Washington Luís, km 235, São Carlos, SP 13565-905, Brazil
**Tania Regina Giraldi,** Universidade Federal de Alfenas (UNIFAL), Rodovia José Aurélio Vilela, 11.999, Poços de Caldas, MG 37715-400, Brazil

Address all correspondence to Graziela Souza at **graziesouza@yahoo.com.br**

(Received 23 January 2022; accepted 19 May 2022; published online: 7 July 2022)

## Abstract

This study aimed to prepare nanostructured ZnO films deposited on FTO substrate by microwave-hydrothermal method. The effects of synthesis time and post-synthesis heat treatment were assessed. ZnO films exhibited a wurtzite structure and a band gap in the range of 3.2 to 3.4 eV. Microwave time influenced film morphology, which varied from lamellar structures (10 min of microwave exposure) to spherical particles (30 min of microwave exposure). Post-synthesis heat treatment removed synthesis residues, increasing film purity and resulting in spherical particles with porous surfaces. These characteristics enhanced the photocatalytic properties of films for degradation of rhodamine B. The findings of this study underscore the importance of microwave conditions in the synthesis of ZnO films with semiconductor properties.

## Introduction

Direct discharge of industrial wastewater into water bodies has caused serious environmental problems worldwide, as these untreated effluents are commonly rich in organic pollutants that can damage aquatic and human life.[1, 2] Photocatalytic oxidation using semiconductor oxides has been widely applied for degradation of industrial contaminants. Photocatalysis consists in the use of radiation to activate oxidation and reduction processes. Compared with other wastewater treatment methods such as microbial degradation and hydrolysis, photocatalysis is a simple and fast technique that can be applied for the removal of recalcitrant organic compounds from aqueous media.[3, 4]

Zinc oxide (ZnO) is an n-type semiconductor with a band gap of about 3.3 eV and promising photocatalytic properties.[4–6] The surface of a ZnO particle is able to absorb photons with an energy equal to or greater than its band gap, promoting photoexcitation of electron–hole pairs and transport of charges.[7] In some studies, ZnO exhibited greater photocatalytic efficiency than the widely used $TiO_2$ catalyst.[6–8] Surface area, crystallinity, defects, and impurities are some of the factors influencing the photocatalytic activity of semiconductor materials, which can be controlled to boost photocatalyst performance.[10]

Semiconductor films have received great attention in photocatalysis because of their several advantages. These materials can be prepared by different techniques, which offers the possibility of selecting the most appropriate synthetic route according to the morphological characteristics desired.[11] Of note, the photocatalytic efficiency of semiconductor films is greatly dependent on factors such as crystal growth and orientation.[12–14] Another advantage of film materials is their easy separation and recovery compared with powder catalysts.[8, 9] Pal et al.[4] synthesized porous ZnO thin films by the sol–gel method using zinc acetate and found that the films had good catalytic efficiency in the decomposition of phenol, chlorophenol, naphthalene, and anthracene to $CO_2$. Yu[15] used a hydrothermal process to synthesize ZnO films deposited on fluorine-doped tin oxide (FTO) substrate. Zinc acetate was dissolved in a 0.75 M solution of ethanolamine and 2-methoxyethanol. The mixture was then agitated at 60°C for 30 min to yield a homogeneous and stable colloid solution. After treatment with the above colloid solution by spin-coating, FTO substrates were annealed at 300°C to afford a ZnO buffer layer. Hydrothermal growth was carried out at 95°C for 12 h in an autoclave with the modified substrates in the precursor solutions. The authors observed that the resulting materials showed different morphologies (nanorods, nanowires, and nanosheets) depending on the precursors used.[15] Jamayaram et al.[12] prepared ZnO films by spray pyrolysis using zinc acetate, zinc chloride, or zinc acetylacetonate as precursor and tested their photocatalytic activity in the degradation of indigo carmine in aqueous medium. The authors reported that all ZnO films showed good

photocatalytic efficiency but those produced from zinc acetate had the best performance.

Synthetic methods and oxide precursors have important implications not only for film morphology and photocatalytic activity but also for process scale-up.[6–8] The current demand for environmentally friendly processes has stimulated research on microwave-assisted hydrothermal synthesis, a method that achieves higher reaction rates in shorter times[16] and at lower temperatures than conventional heat-based methods, providing high yields and resource savings. Furthermore, process parameters can be adjusted to control particle distribution, size, and morphology.[17] Huang et al.[16] synthesized ZnO films by a microwave-assisted method and found that microwave irradiation promoted induced nucleation and created a 3D morphology of unique complexity.

Although the synthesis of ZnO thin films by microwave-assisted hydrothermal methods is not widely used, there are some reports of this approach in the literature. Aksoy et al.[18] obtained ZnO films deposited on FTO substrate. For this, aqueous solutions of zinc acetate dihydrate and sodium hydroxide were prepared as precursor materials. These solutions were irradiated with microwaves at 300 W for 10 min. Then, ZnO films were prepared by squeezing the paste onto FTO substrate using plastic tapes, followed by annealing for 1 h at 400°C in air and cooling to room temperature. The photoelectrochemical properties of these films were evaluated. Chen et al.[19] produced well-aligned ZnO nanorods rapidly grown on an indium tin oxide (ITO) substrate (seed layer) by a microwave-assisted hydrothermal chemical route. Optimal growth conditions were obtained by modulating the $H_2$ plasma pretreatment time of the seed layer and the synthesis time of ZnO nanorods. The results showed that the alignment and growth rate of ZnO nanorods depend on the physical characteristics and roughness of the seed layer. Richardson et al.[20] obtained ZnO films by deposition of epitaxial ZnO using microwave heating. This method allowed for much higher ZnO nucleation and growth rates than those observed with conventional heating. Using this technique, the authors were able to deposit a several micron-thick epitaxial ZnO film in a few minutes. Filip et al.[21] successfully obtained 1D (nanorods) and 2D (nanoplates) ZnO nanostructures with homogeneous distribution and orientation perpendicular to ITO-coated glass substrate seeded with ZnO by a microwave-assisted hydrothermal method. By modifying the type and duration of the post-deposition treatment of the seed layer, it was possible to achieve significant changes in the structure and morphology of ZnO nanostructures grown on annealed seed layers.

Post-synthesis heat treatment may be used to increase optical transmittance and enhance photocatalytic properties. Bouhssira et al.[22] demonstrated that heat treatment interferes with the formation of ZnO phases. The authors obtained thin films deposited by thermal evaporation of ZnO powder. As-deposited films were dark brown and rich in zinc and exhibited low transmittance. Films were annealed in air at temperatures ranging from 100 to 400°C. It was observed that film oxidation began at 250°C. XRD peaks associated with ZnO emerged and those related to zinc decreased with increasing temperature. At 300°C, zinc was totally oxidized and films became completely transparent. A decrease in grain boundary density was also observed, leading to reduced mobility of charge carriers and increased band gap.

At mild temperatures, heat treatment typically results in small particle sizes and large surface areas. High-temperature treatments promote an increase in particle size but have the benefit of removing synthesis residues and metastable phases, increasing crystallinity, which is a determining factor for photocatalytic performance.[23]

This study aimed to synthesize ZnO films deposited on FTO substrate by microwave-assisted hydrothermal method and assess the effects of synthesis time and post-synthesis heat treatment on photocatalytic properties, surface characteristics, and morphology. Elucidation of this method can contribute to its use in film formation under controlled conditions. There are no literature reports on the properties of semiconductors prepared under the conditions used in this study.

## Results and discussion

Figure 1 shows the XRD, FTIR, and DRS patterns of film samples. XRD patterns of FTO substrate and ZnO-10 and ZnO-30 with and without heat treatment revealed peaks characteristic of FTO ($SnO_2$, JCPDS 77-450) and ZnO (JCPDS 33-1451) [Fig. 1(a)].

XRD spectra of samples not subjected to heat treatment showed additional peaks, suggesting the presence of residues from the synthesis process or possible metastable phases. FTIR spectra of untreated samples revealed the presence of hydroxylated groups characterized by a broad band at 3100–3500 $cm^{-1}$, methyl groups at 2984 and 2885 $cm^{-1}$, and carboxylate groups at 1572, 1406, and 800–900 $cm^{-1}$ [Fig. 1(c)].[24] Wojnarowicz et al.[25] reported that solvothermal synthesis of ZnO using ethylene glycol and water resulted in the formation of unstable intermediates, such as $Zn_5(OH)_8(CH_3COO)_2{\cdot}xH_2O$, which served as an esterification catalyst during the reaction. After heat treatment in a muffle furnace, however, films exhibited better-defined peaks and greater crystallinity, as the intermediate phase was fully converted to ZnO. In the current samples, the wurtzite ZnO phase was identified in XRD patterns and found to be successfully crystallized. No other secondary phase was observed. This polymorph has a zincite crystal prototype with hexagonal symmetry and a $P6_3mc$ space group,[26] space group no. 186 according to the International Union of Crystallography classification.[27] XRD patterns had peaks characteristic of wurtzite ZnO and cassiterite ($SnO_2$). The $SnO_2$:F thin layer has a rutile-type tetragonal structure ($P4_2/mnm$, no. 136).[27–29] This conductive layer was sufficiently thick to be identified in the diffractograms and attenuate background noise and halo from the glass substrate. The absence of peaks not related to wurtzite and cassiterite indicates that no other secondary phase was crystallized and that reactions between SnO:F and ZnO layers did not occur in detectable quantities.

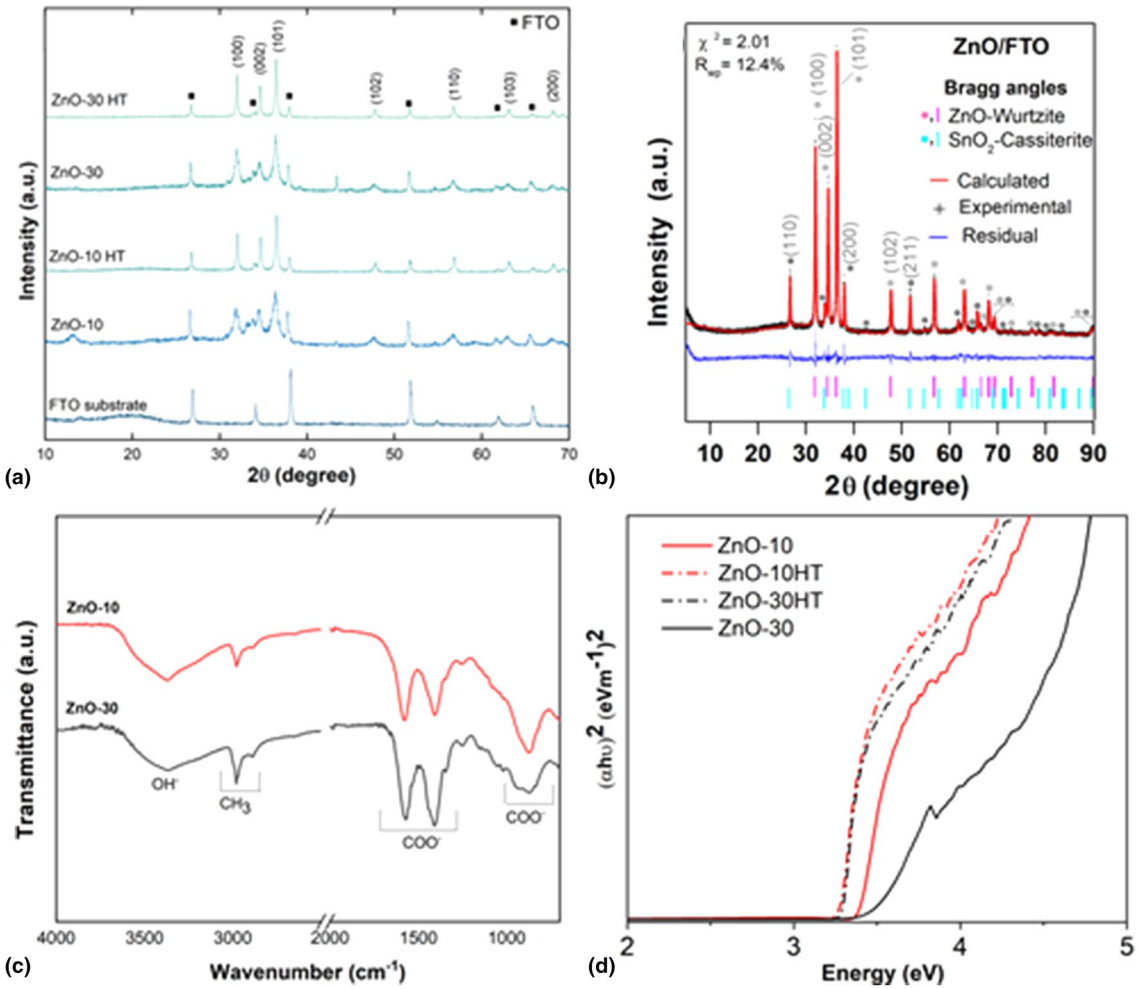


**Figure 1.** (a) X-ray diffractograms of ZnO films; (b) Rietveld refinement of ZnO-30HT. The main diffraction peaks of each phase are highlighted; (c) Fourier transform infrared spectra of ZnO-10 and ZnO-30; (d) Tauc plots of ZnO films.

This factor is corroborated by the convergence of the Rietveld refinement, as illustrated in Fig. 1(b). Interestingly, cassiterite exhibited preferred orientation along the (200) plane, attributed to the columnar nature of the $SnO_2$:F layer, favoring diffraction from this plane.

The UV–Vis spectroscopy technique was used to examine the optical properties of ZnO films. Figure 1(d) shows the optical energy plots for direct gap determination ($n = ½$) from the intercept of $(\alpha h\nu)^2$ vs $h\nu$. The Kubelka–Munk model was applied to DRS data to convert the diffuse reflectance $R$ into a parameter called $F(R)$, which is proportional to the absorption coefficient $\alpha$. That is, the parameter $F(R)$ has a similar behavior to $\alpha$ and allows determining the band gap of the material through Tauc plots. The band gap of films ranged from 3.2 to 3.4 eV. Heat-treated samples had a discreetly lower band gap energy than untreated samples. It is possible that the higher crystallinity of heat-treated samples led to a decrease in band gap energy.

Figure 2 shows the SEM images of heat-treated and untreated samples. The surface of ZnO-10 had a lamellar morphology. A longer reaction time altered the morphological characteristics of films. ZnO-30 exhibited spherical particles of about 45 nm agglomerated into irregular shapes, similar to the irregular morphology observed in ZnO-10. Heat treatment at 600°C [Fig. 2(b), (d)] resulted in the formation of large clusters with a mean size of 400 nm. Agglomerate formation contributed to high surface roughness and unevenness. ZnO-10HT exhibited 80 nm particles and large agglomerates with a mean size of up to 1 µm. Agglomerates formed by heat treatment for short periods (ZnO-10HT) exhibited open voids, probably formed by the expel of gases from decomposition of organic intermediates.

Open voids may contribute to the exposure of photocatalyst-active sites to reactive media. On the other hand, prolonged heat treatment (ZnO-30HT) closed the voids, as heat reduces the exposed area and consequently the surface energy per mass. The

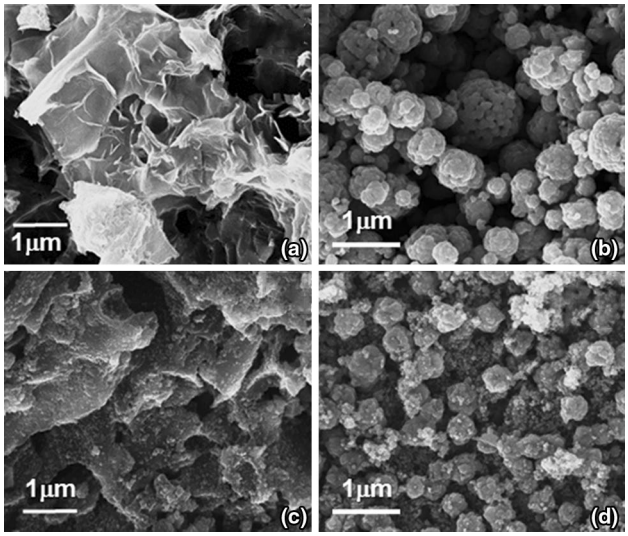


**Figure 2.** SEM-FEG micrographs of the ZnO films: (a) ZnO-10, (b) ZnO-10HT, (c) ZnO-30 and (d) ZnO-30HT.

reduction of voids was likely responsible for the reduction in particle cluster sizes.

The photocatalytic activity of films was assessed by Rhodamine B (RhB) degradation assays, as shown in Fig. 3. Untreated samples had similar photocatalytic activities, affording 25% dye degradation. This finding indicates that surface morphology did not influence photocatalytic activity, as ZnO-10 had a lamellar structure and ZnO-30 exhibited spherical particles with an average size of 48 nm. Heat treatment increased photocatalytic activity to up to 50% dye degradation. ZnO-10HT and ZnO-30HT were composed of large particle clusters, although cluster size differed between samples (400 nm in ZnO-30HT and 1000 nm in ZnO-10HT). Heat-treated samples also showed high surface roughness and irregularity, characteristics that might have contributed to RhB adsorption and, consequently, photocatalytic activity. The improvement in photocatalytic activity with heat treatment may also be attributed to the increase in active sites, as intermediate compounds (evidenced by XRD) were decomposed and converted to ZnO with prominent crystallinity [Fig. 1(a), (b)]. Therefore, the effects of adsorption of intermediate compounds onto the film surface seem to be more relevant than those of particle size.

A kinetic study was made based on the linearization of a pseudo-first order applied to a batch system. For a diluted system, the photocatalytic reaction follows a pseudo-first-order kinetics (Eqs. 1 and 2):

$$r = k'C \tag{1}$$

and also:

$$r = -\frac{dC}{dt} \tag{2}$$

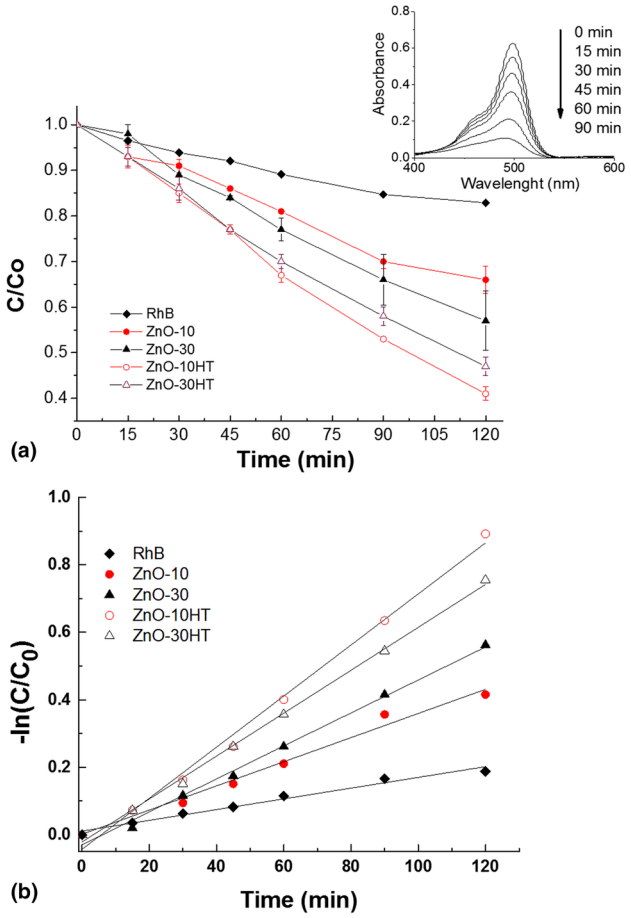


**Figure 3.** Kinetic study of the photocatalytic degradation of rhodamine B. (a) Decolorization as a function of reaction time; (b) first-order kinetics of degradation by ZnO thin films.

in which $r$ is the rate of reaction (discoloration of the dye), $k'$ the apparent reaction constant, and $C$ the concentration of the dye at a time $t$. The minus signal indicates consume of the dye.

Equation 3 combines the Eqs. 1 and 2 to form an equation that represents the variation of the dye's concentration according to the time:

$$-\frac{dC}{dt} = k'C \tag{3}$$

To resolve Eq. 3, the following boundary conditions are considered for integration: at a time $t$ the dye will have a concentration $C$, and at the initial time ($t$=0 min) the dye will have the initial concentration $C_0$. The results of integration lead to the Eq. 4:

$$\ln\left(\frac{C_0}{C}\right) = k't \tag{4}$$

Equation 4 is the integrated law for the kinetic of the dye consumption. Equation 4 can also be written in different ways, as presented in Eq. 5:

$$-\ln\left(\frac{C}{C_0}\right) = k't \tag{5}$$

Thus, making a linearization of Eq. 5 by plotting $-\ln\left(C/C_0\right)$ versus $t$, the $k'$ is measured as the slope of linearization.

Furthermore, these equations allow to obtain the half-life time ($t_{1/2}$). This parameter is based on the same integrated law (Eq. 4). This parameter is the time $t$ when the concentration of the dye reaches 50% of the initial value, that is, $C = 0.5\ C_0$. Substituting this information in Eq. 4 and reorganizing the equation as the function of $t$ (Eq. 6):

$$t_{1/2} = \frac{\ln 2}{k'} \tag{6}$$

where $t_{1/2}$ is the half-time life considering a pseudo-first-order kinetic and a batch reaction. Briefly, as high $k'$ is, as low $t_{1/2}$. Lower values for $t_{1/2}$ represent that 50% of the initial dye is more rapidly consumed and represents faster photocatalytic degradation and better photocatalytic potential for the photocatalyst used.

Thus, Fig. 3(b) shows the curve of $-\ln(C/C_0)$ versus time, obtained from Fig. 3(a) and Eq. 1. The curves show that the reaction followed first-order kinetics for all samples. The mean values of $k'$, $R^2$, and half-life are described in Table I.

The kinetic study revealed that, for samples prepared by microwave treatment only (ZnO-10 and ZnO-30), an increment in synthesis time increased $k'$. As expected, $t_{1/2}$ was reduced, given that RhB was consumed faster. The increase in photocatalytic activity is attributed to the increase in ZnO crystallinity and reduction in intermediate products promoted by extended microwave time. Complementary heat treatment for a short period further enhanced photocatalytic performance: ZnO-10HT had a considerably higher $k'$ and lower $t_{1/2}$ than the other samples. This result is mainly attributed to the conversion of intermediate phases into photoactive ZnO. However, it should be noted that an increase in heat treatment time is not a guarantee of increased performance. In fact, photocatalytic activity was impaired by a longer heat treatment time (ZnO-30HT), leading to reduced $k'$ and increased $t_{1/2}$. This result can be attributed to the closing of voids of particle clusters promoted by extended heat treatment, which may reduce exposed surface area, thereby decreasing photocatalytic performance.

**Table I.** First kinetic values of $k'$, $t_{1/2}$ and $R^2$ for each sample and blank (RhB).

| Parameters | RhB | ZnO-10 | ZnO-30 | ZnO-10HT | ZnO-30HT |
|---|---|---|---|---|---|
| $k'$ ($10^{-3}$ min$^{-1}$) | 1.59 | 3.58 | 6.36 | 7.57 | 4.89 |
| $R^2$ | 0.98 | 0.98 | 0.99 | 0.99 | 0.99 |
| $t_{1/2}$ | 435.8 | 193.6 | 141.7 | 91.5 | 109 |

## Conclusion

ZnO films were obtained by microwave-assisted hydrothermal method and applied as photocatalysts in RhB degradation. The influence of synthesis plateau time (10 and 30 min) and post-synthesis heat treatment (at 600°C) on the structural and optical properties of films was examined. Films had a wurtzite phase and a band gap of 3.2 to 3.4 eV. Films not subjected to heat treatment exhibited metastable phases or synthesis residues. Such residues were easily converted to ZnO by heating at 600°C in a muffle furnace. The presence of residues on the film surface led to a reduction in the efficiency of active sites, consequently decreasing photocatalytic activity. Heat-treated films were composed of large particle agglomerates, resulting in an uneven, rough surface. These characteristics further contributed to improving the photocatalytic properties of ZnO films. Thin films produced by a microwave method and posteriorly treated for short periods at 600°C demonstrated the best photocatalytic results, attributed to the complete conversion of intermediates into photoactive ZnO and proper agglomerate morphology. These factors improved the number of photoactive phases in the catalyst and active sites exposed to reactive media, key characteristics for enhanced photocatalytic performance.

## Methods

### *Synthesis of ZnO film*

First, FTO substrate was prepared, cut into 1 × 1 cm pieces, and subjected to a hydrophilization step.[30] This process increases adhesion between substrate and film-forming solution. An alkaline hydrophilization solution was prepared by mixing ammonium hydroxide ($NH_4OH$), hydrogen peroxide ($H_2O_2$), and deionized water at a molar ratio of 6:1:1 under magnetic agitation (100 rpm) at 70°C for 10 min. The substrates were immersed in this solution at 70°C and 100 rpm for 15 min, rapidly washed with ultrapure acetone to remove excess hydrophilization solution, and oven-dried for 10 min at 100°C.

ZnO films were prepared according to the procedures described by Wojnarowicz.[31] Briefly, 1.665 g of zinc acetate dihydrate ($Zn(CH_3COO)_2.2H_2O$ Synth), 25.00 mL of ethylene glycol ($HOCH_2CH_2OH$, Synth), and 0.150 mL of deionized water were added to a beaker and maintained under magnetic stirring at 100 rpm and 70°C for 20 min. After this period, the solution was transferred to an Erlenmeyer flask containing FTO substrate. The flask was sealed with a rubber stopper and treated in a microwave digestion system (MARS 6™, CEM) at 600 W with a heating ramp of 5 min to 180°C. The plateau time varied from 10 to 30 min. Upon completion of the reaction, one part of the samples was oven-dried at 100°C for 30 min. The other part was subjected to heat treatment at 600°C for 2 h using a heating rate of 1°C/min. Oxide films were coded as ZnO-t, where $t$ stands for the plateau time during microwave synthesis. Heat-treated samples were additionally coded as HT.

### Characterization

Film structure and morphology were assessed by X-ray diffractometry (XRD) on a Bruker D8 Advance ECO diffractometer in the $2\theta$ range of 20°–90° at a scanning rate of 4.5°/min. Rietveld refinement was evaluated using GSAS software with the EXPGUI interface. Yttrium oxide ($Y_2O_3$) (99.99%, Sigma–Aldrich) was analyzed under the same conditions and used as standard. The instrumental parameters for Rietveld refinement were acquired by Le Bail refinement of the $Y_2O_3$ diffractogram. Fourier transform infrared (FTIR) analyses (Agilent Technologies, Cary 360) were performed on ZnO-10 and ZnO-30 samples, using a wavelength range of 600 to 4000 $cm^{-1}$ at a resolution of 4 $cm^{-1}$. Film morphology was determined by field-emission scanning electron microscopy (FE-SEM) on a FEI Magellan 400L apparatus. For band gap determination, diffuse reflectance spectra (DRS) in the ultraviolet—visible—near-infrared (UV–Vis–NIR) region (200–1200 nm) were obtained using a Shimadzu UV–Vis equipment in the diffuse reflectance mode at room temperature. The band gap energy was estimated by applying the Kubelka–Munk model[32] and by constructing Tauc plots.

### Photocatalysis assay

Photocatalytic activity was investigated by evaluating Rhodamine B (RhB) photodegradation. Films were submerged in 15 mL of 5 mg/L RhB (Contemporary Chemical Dynamics) in Petri dishes and placed in a bench-scale photocatalytic reactor equipped with four 15 W Philips mercury lamps (UV-C, 254 nm) at room temperature. Dye reduction was determined by monitoring color removal during 120 min of reaction using a spectrophotometer (Cary 60 UV–Vis, Agilent). Relative RhB concentration was quantified by measuring absorbance at 554 nm.[33] A solution of RhB only (without the photocatalyst) was subjected to the same procedures to assess the occurrence of photolysis.

## Acknowledgments

The authors thank CNPq and FAPEMIG for the financial support. They also thank the Laboratory of Structural Characterization (LCE/DEMa/UFSCar) for providing facilities.

## Data availability

The authors state that the raw data used in this work is available in the Mendeley Data repository.

## Declarations

## Competing interests

The authors declare that they have no knowledge of competing financial interests or personal relationships that could have influenced the work reported in this paper.

## References

1. Q.I. Rahman, M. Ahmad, S.K. Misra, M. Lohani, Mater. Lett. (2013). https://doi.org/10.1016/j.matlet.2012.09.044
2. K. Byrappa, A.K. Subramani, S. Ananda et al., Mater. Sci. (2006). https://doi.org/10.1007/BF02914073
3. A. Di Mauro, M.E. Fragalà, V. Privitera, G. Impellizzeri, Mater. Sci. Semicond. Process. (2017). https://doi.org/10.1016/j.mssp.2017.03.029
4. B. Pal, M. Sharon, Mater. Chem. Phys. (2002). https://doi.org/10.1016/S0254-0584(01)00514-4
5. A.A. Aal, S.A. Mahmoud, A.K. Aboul-Gheit, Mater. Sci. Eng. C (2009). https://doi.org/10.1016/j.msec.2008.07.035
6. Y. Mao, Y. Li, Y. Zou et al., Ceram. Int. (2019). https://doi.org/10.1016/j.ceramint.2018.10.054
7. S.B.A. Hamid, S.J. Teh, C.W. Lai, Catalysts (2017). https://doi.org/10.3390/catal7030093
8. H.L. Liu, T.C.K. Yang, Process Biochem. (2003). https://doi.org/10.1016/S0032-9592(03)00084-0
9. J. Xie, H. Wang, M. Duan, L. Zhang, Appl. Surf. Sci. (2011). https://doi.org/10.1016/j.apsusc.2011.01.105
10. S. Klubnuan, S. Suwanboon, P. Amornpitoksuk, Opt. Mater. (2016). https://doi.org/10.1016/j.optmat.2016.01.045
11. V.K. Jayaraman, A. Hernández-Gordillo, M. Bizarro, Mater. Sci. Semicond. Process. (2018). https://doi.org/10.1016/j.mssp.2017.11.015
12. A. Ramirez-Canon, M. Medina-Llamas, M. Vezzoli, D. Mattia, Phys. Chem. (2018). https://doi.org/10.1039/C7CP07984B
13. N. Talebian, M.R. Nilforoushan, R. Ramazan Ghasem, J. Sol-Gel Sci. Technol. (2012). https://doi.org/10.1007/s10971-012-2825-4
14. L. Wang, Y. Zheng, X. Li et al., Thin Solid Films (2011). https://doi.org/10.1016/j.tsf.2011.02.070
15. J. Yu, B. Huang, X. Qin et al., Appl. Surf. Sci. (2011). https://doi.org/10.1016/j.apsusc.2011.01.039
16. J. Huang, C. Xia, L. Cao, X. Zeng, Mater. Sci. Eng. B (2008). https://doi.org/10.1016/j.mseb.2008.05.014
17. F. Al-Hazmi, N.A. Aal, A.A. Al-Ghamdi et al., J. Electroceramics. (2013). https://doi.org/10.1007/s10832-013-9846-4
18. S. Aksoy et al., J. Mol. Struct. (2019). https://doi.org/10.1016/j.molstruc.2019.04.040
19. M. Chen et al., J. Nanosci. Nanotechnol. (2015). https://doi.org/10.1166/jnn.2015.11429
20. J.J. Richardson, F.F. Lange, J. Mater. Chem. (2011). https://doi.org/10.1039/c0jm02907f
21. A. Filip et al., Optik (2020). https://doi.org/10.1016/j.ijleo.2020.164372
22. N. Bouhssira, S. Abed, E. Tomasella et al., Appl. Surf. Sci. (2006). https://doi.org/10.1016/j.apsusc.2005.12.134
23. T.R. Giraldi, G.V.F. Santos, V.R. Mendonça et al., J. Nanosci. Nanotechnol. (2011). https://doi.org/10.1166/jnn.2011.3801
24. R.M. Silverstein, G.C. Bassler, T.C. Morrill, *Spectrometric Identification of Organic Compounds*, 5th edn. (Wiley, New York, 1991)
25. J. Wojnarowicz, T. Chudoba, I. Koltsov et al., Nanotechnology (2018). https://doi.org/10.1088/1361-6528/aaa0ef
26. M. Schreyer, L. Guo, S. Thirunahari, F. Gao, M. Garland, J. Appl. Crystallogr. (2014). https://doi.org/10.1107/S1600576714003379
27. H. Arnold, M.I. Aroyo, E.F. Bertaut, *International Tables for Crystalography - Vol. A: Space-Group Symmetry*, 5th ed. (Springer, Dordrecht, 2005)
28. B.H. Toby, Powder Diffr. (2006). https://doi.org/10.1154/1.2179804
29. H. Seki, N. Ishizawa, N. Mizutani, M. Kato, J. Ceram. Assoc. Jpn. (1984). https://doi.org/10.2109/jcersj1950.92.1064_219
30. V.P. Ulin, N.V. Ulin, F.Y. Soldatenkov, A.V. Semenov, A.V. Bobyla, Semiconductor (2014). https://doi.org/10.1134/S1063782614090243
31. J. Wojnarowicz, T. Chudoba, S. Gierlotka et al., Cryst (2018). https://doi.org/10.3390/cryst8040179
32. Í.G. Gonçalves, C.O. Petter, Rem. Ver. Esc. Minas. (2007). https://doi.org/10.1590/s0370-44672007000300009
33. J.A. Oliveira, A.E. Nogueira, M.C.P. Gonçalves et al., Appl. Surf. Sci. (2018). https://doi.org/10.1016/j.apsusc.2017.10.110